Specialty area: Emerging Brain Techniques

Highlights:
1. QSM quantifies magnetic properties of tissue.
2. QSM can be acquired with gradient echo sequences;
3. QSM is 3D and of high resolution;
4. QSM quantifies myelination, iron deposition and calcification;
5. STI images tissue microstructure and fiber orientation.

CNS Quantitative Susceptibility Mapping (QSM)

[1, 2] Chunlei Liu, PhD,
Email: chunlei.liu@duke.edu
[1] Brain Imaging and Analysis Center, [2] Department of Radiology, Duke University, Durham, NC

Target audience: physicists, neuroscientists and clinicians interested in learning the principles and applications of QSM.

PURPOSE

Phase and magnetic susceptibility maps derived from gradient-echo MRI provides a unique contrast among various cortical and sub-cortical gray and white matter tissues (1-9). The excellent tissue contrast has been largely attributed to the sensitivity of magnetic susceptibility to the spatial variations of molecular or cellular components, especially iron and myelin that are of different magnetic properties compared to bulk water (3,8,10-15). The objectives of the lecture are to understand the underlying concepts of QSM; to explain the basic acquisition and processing protocols of QSM; to recognize the benefits and pitfalls of QSM in CNS applications.

METHODS

Overview

Magnetic susceptibility is a physical property that reflects how a substance changes the magnetic field. Magnetic susceptibility of a material, noted by χ, is equal to the ratio of the magnetization M within the material to the applied magnetic field strength H, i.e. $\chi = M/H$. This definition of susceptibility is in fact the volume susceptibility or bulk susceptibility. In MRI images, it is the volume susceptibility involving the magnetism (a dipole moment) per voxel. Magnetic materials are classically classified as diamagnetic, paramagnetic, or ferromagnetic on the basis of their susceptibilities. Biological tissues can be either diamagnetic or paramagnetic depending on its molecular contents and microstructure.

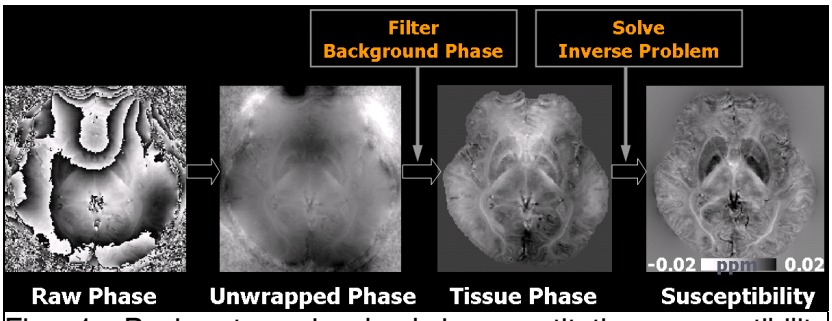

Fig. 1. Basic steps involved in quantitative susceptibility mapping (QSM)

Susceptibility is usually measured with gradient-echo sequences. In GRE images, variations of tissue magnetic susceptibility result in signal cancellation in the magnitude and frequency shift in the phase. While magnitude images are routinely used in MRI, phase images are typically severely corrupted by phase wraps and overwhelmed by non-tissue-specific background phases. Quantifying tissue magnetic susceptibility from these phase images involves three basic steps (Fig. 1): 1. 3D phase unwrapping, 2. separating background and tissue phase, 3. solving an ill-posed deconvolution problem. These processes can be accomplished in freely available software such as STI Suite (16).

Sequences for acquiring phase images

The most commonly used sequence for measuring phase and susceptibility is the spoiled-gradient-recalled-echo (SPGR or GRE) sequence. The phase of GRE images gives a measure of local frequency offset which in turn can be used to calculate susceptibility quantitatively. The magnitude of a series of multi-echo GRE images is used to estimate the T2* relaxation time using a single exponential or multi-exponential fitting. The flip angle, TE and TR can be optimized to improve SNR (17). Higher readout bandwidth can be used to reduce artifacts and T2* decay induced blurring.

Processing phase images

Two key steps are typically required in order to visualize tissue susceptibility contrast and for susceptibility quantification: phase unwrapping and background phase removal. Several methods have become readily available and have so far served the need for susceptibility mapping. These methods include, for example, path-based method and Laplacian based method (1). Once the phase is unwrapped, underlying tissue contrast is usually covered by large background phases that are generated from sources outside the brain. These large background phases can be removed with several methods, e.g, the spherical-mean-value based filtering (SHARP) (18), dipole field fitting (PDF) (19) and integrated HARPERELLA (16).

Susceptibility quantification

Quantitative susceptibility values can be calculated from background-phase removed frequency shift maps by solving a linear equation. The relationship between frequency shift f(r) and the spatially distributed susceptibility $\chi(r)$ is expressed in a Fourier transform as

$$\Delta f = FT^{-1}\left[\frac{1}{3}\boldsymbol{\chi}(\mathbf{k}) - \frac{k_z^2\boldsymbol{\chi}(\mathbf{k})}{k^2}\right]\gamma\mu_0 H_0 \qquad [1]$$

Here $\chi(k)$ is the 3D Fourier transform of $\chi(r)$ and k is the spatial frequency vector. The equation can be inverted in the k-space. However, when $3k_z^2 = k^2$, the coefficient is zero prohibiting a direct inversion. Several viable solutions have been proposed. A simple strategy makes a threshold of the coefficients by replacing them with a small number whenever they are below that value. Other strategies utilize, e.g., regularization (6-7), multiple angle acquisition (4), LSQR algorithm (1) and compressed sensing (20).

RESULTS

Magnetic susceptibility of tissue has recently been shown to reflect organ's molecular composition, structure, function and disease state. For example, phase contrast has revealed unprecedented spatial details of brain anatomy *in vivo* (2-3,21). QSM is enabling noninvasive and *in vivo* measurements of oxygen saturation and iron deposition in stroke, multiple sclerosis, Parkinson's and Alzheimer's diseases, and other neurological disorders and diseases (18,21-46). Further, QSM offers a new contrast mechanism for studying properties of nerve bundles including myelination and fiber tract orientation (15,39,47-56).

Quantification of iron concentration

Gradient echo signal phase was increasingly applied to assess iron contents in deep brain nuclei. QSM showed great promise for assessment of deep brain nuclei, e.g. it can reliably differentiate sunthalamus nuclei from the adjacent substantia nigra (57). Recently, emerging evidence suggests susceptibility is also linearly correlated with iron content in the basal ganglia nuclei (58-60). Both $R2^*$ and susceptibility are related to microscopic magnetic field perturbation. While $R2^*$ reflects the spectral width of field inhomogeneity, susceptibility is derived from the mean field shift. The good linearity between susceptibility and $R2^*$ and the similar temporal

parameters suggest that magnetic susceptibility may be potentially used as a biomarker of brain iron deposits in gray matter. With standard multi-echo gradient-echo sequences, $R2^*$ and susceptibility can be measured simultaneously without scan time penalty.

Quantification of demyelination and dysmyelination

Recent studies have established that magnetic susceptibility of brain white matter is closely related to myelin content. Liu et al reported that the loss of myelin sheath around axons in a transgenic dysmyelinating shiverer mice led to almost complete loss of phase and susceptibility contrasts between gray and white matter (15). These results suggest that myelin is the predominant source of susceptibility difference between deep gray and white matter. Lee et al also showed that frequency contrast are substantially reduced in mice with significant myelin loss induced by a cuprizone diet (52). Together, these studies indicated the potential value of QSM for the study of myelination in the white matter.

QSM of brain development and aging

Myelination and iron deposition in the brain evolve spatially and temporally. This evolution reflects an important characteristic of normal brain development and ageing. Li et al assessed the changes of regional susceptibility in the human brain *in vivo* by examining the developmental and ageing process from 1 to 83 years of age (61). The evolution of magnetic susceptibility over the lifespan was found to display differential trajectories between the gray and the white matter. In both cortical and subcortical white matter, an initial decrease followed by a subsequent increase of magnetic susceptibility was observed, which could be fitted by a Poisson curve. In the gray matter, including the cortical gray matter and the iron-rich deep nuclei, magnetic susceptibility displays a monotonic increase, which can be described with an exponential growth. The rate of change varies according to functional and anatomical regions of the brain. In another study, Argyridis et al assessed QSM and susceptibility anisotropy changes in mouse brains (62).

Imaging white matter microstructure and connectivity

Magnetic susceptibility of white matter is also anisotropic (8,63). To measure the anisotropy of magnetic susceptibility, the method of susceptibility tensor imaging (STI) has been used (8). A recent study also explored the capability of STI for tracking neuronal fibers in 3D in the mouse brain ex vivo (64). In large fiber bundles, the orientation determined by STI was found to be comparable to that by diffusion tensor imaging (DTI) of diffusion anisotropy. A recent study suggested that the susceptibility anisotropy in brain tissue mainly originates from myelin, and the cylindrically aligned lipid molecules in myelin are likely the main source of the MRI-determined susceptibility anisotropy (65).

However, this experimental procedure of STI requires rotating the object or the magnetic field. A p-space method was recently developed to measure higher-order frequency variations based on a single image acquisition without rotating the object or the magnet (48). This method utilized a multipole analysis of the MRI signal in a sub-voxel Fourier spectral space termed “p-space” for short. By sampling the p-space with pulsed field gradients or by shifted image reconstruction, a set of dipole and quadrupole susceptibility tensors can be measured. This p-space approach may provide a powerful method for studying tissue microstructure and brain connectivity in vivo and non-invasively.

DISCUSSION

QSM is a deconvolution tool for analyzing MRI phase allowing the study of tissue magnetic susceptibilities (66-67) and their relations with organ structures, functions and diseases. QSM has shown a wide range of scientific and clinical applications (1,4,8-9,15,17,46,68-82). QSM is enabling quantitative functional connectivity and biophysical studies in neuroimaging, providing

an important tool for neuroscience and neuroengineering. Understanding, diagnosing, and treating neurological disorders can benefit from QSM measurements of white matter tracts and iron deposition. In the clinics, QSM can be applied for risk assessment and therapy monitoring by measuring iron deposition, demyelination, and connectivity disruption in neurodegenerative diseases, including Alzheimer's disease, Parkinson's disease, and multiple sclerosis; measuring oxygen level in ischemic stroke patients; measuring microbleeds in traumatic brain injury and in patients at risk of hemorrhages; differentiating calcification from iron deposition; and characterizing atherosclerotic plaque.

While QSM has shown to be valuable in a wide range of applications, it will benefit from further technical refinement. Existing methods need to be evaluated systematically under a variety of experimental conditions and quantitative susceptibility values need to achieve high degrees of consistency. The lack of an absolute measure of susceptibility may be a fundamental shortfall of these techniques that may ultimately limit the utility of susceptibility mapping if not addressed properly.

Quantifying magnetic susceptibility is also complicated by the existence of multiple sources to the frequency contrast. Some sources may not even be related to susceptibility. For example, both chemical shift and proton exchange affect the measured frequency. Partial volume effect and tissue compartmentalization may also render Eq. [1] inaccurate and incorrect. These confounding factors may make it difficult to interpret the physical and biological meanings of the "quantitative" susceptibility maps.

CONCLUSION: QSM has been quickly established as a high-resolution and quantitative imaging technique for the CNS. Image acquisition for QSM is relatively simple and is compatible with all modern MRI scanners. QSM algorithms are becoming increasingly mature. QSM is poised to become an important tool for studying the CNS.

REFERENCES:

1. Li W, Wu B, Liu C. Quantitative susceptibility mapping of human brain reflects spatial variation in tissue composition. Neuroimage 2011;55(4):1645-1656.
2. Rauscher A, Sedlacik J, Barth M, Mentzel HJ, Reichenbach JR. Magnetic susceptibility-weighted MR phase imaging of the human brain. AJNR Am J Neuroradiol 2005;26(4):736-742.
3. Duyn JH, van Gelderen P, Li TQ, de Zwart JA, Koretsky AP, Fukunaga M. High-field MRI of brain cortical substructure based on signal phase. Proc Natl Acad Sci U S A 2007;104(28):11796-11801.
4. Liu T, Spincemaille P, de Rochefort L, Kressler B, Wang Y. Calculation of susceptibility through multiple orientation sampling (COSMOS): a method for conditioning the inverse problem from measured magnetic field map to susceptibility source image in MRI. Magn Reson Med 2009;61(1):196-204.
5. Shmueli K, de Zwart JA, van Gelderen P, Li TQ, Dodd SJ, Duyn JH. Magnetic susceptibility mapping of brain tissue in vivo using MRI phase data. Magn Reson Med 2009;62(6):1510-1522.
6. de Rochefort L, Liu T, Kressler B, Liu J, Spincemaille P, Lebon V, Wu J, Wang Y. Quantitative susceptibility map reconstruction from MR phase data using bayesian regularization: validation and application to brain imaging. Magn Reson Med 2010;63(1):194-206.
7. Kressler B, de Rochefort L, Liu T, Spincemaille P, Jiang Q, Wang Y. Nonlinear Regularization for Per Voxel Estimation of Magnetic Susceptibility Distributions From MRI Field Maps. IEEE Trans Med Imaging 2010;29(2):273-281.
8. Liu C. Susceptibility tensor imaging. Magn Reson Med 2010;63(6):1471-1477.
9. de Rochefort L, Brown R, Prince MR, Wang Y. Quantitative MR susceptibility mapping using piece-wise constant regularized inversion of the magnetic field. Magn Reson Med 2008;60(4):1003-1009.
10. Haacke EM, Xu Y, Cheng YC, Reichenbach JR. Susceptibility weighted imaging (SWI). Magn Reson Med 2004;52(3):612-618.
11. Haacke EM, Ayaz M, Khan A, Manova ES, Krishnamurthy B, Gollapalli L, Ciulla C, Kim I, Petersen F, Kirsch W. Establishing a baseline phase behavior in magnetic resonance imaging to

determine normal vs. abnormal iron content in the brain. J Magn Reson Imaging 2007;26(2):256-264.
12. Haacke EM, Makki M, Ge Y, Maheshwari M, Sehgal V, Hu J, Selvan M, Wu Z, Latif Z, Xuan Y, Khan O, Garbern J, Grossman RI. Characterizing iron deposition in multiple sclerosis lesions using susceptibility weighted imaging. J Magn Reson Imaging 2009;29(3):537-544.
13. Kirsch W, McAuley G, Holshouser B, Petersen F, Ayaz M, Vinters HV, Dickson C, Haacke EM, Britt Iii W, Larsen J, Kim I, Mueller C, Schrag M, Kido D. Serial Susceptibility Weighted MRI Measures Brain Iron and Microbleeds in Dementia. J Alzheimers Dis 2009.
14. Yao B, Li TQ, Gelderen P, Shmueli K, de Zwart JA, Duyn JH. Susceptibility contrast in high field MRI of human brain as a function of tissue iron content. Neuroimage 2009;44(4):1259-1266.
15. Liu C, Li W, Johnson GA, Wu B. High-field (9.4 T) MRI of brain dysmyelination by quantitative mapping of magnetic susceptibility. Neuroimage 2011;56(3):930-938.
16. Li W, Avram AV, Wu B, Xiao X, Liu C. Integrated Laplacian-based phase unwrapping and background phase removal for quantitative susceptibility mapping. NMR Biomed 2013.
17. Wu B, Li W, Avram AV, Gho SM, Liu C. Fast and tissue-optimized mapping of magnetic susceptibility and T2* with multi-echo and multi-shot spirals. Neuroimage 2012;59(1):297-305.
18. Schweser F, Sommer K, Deistung A, Reichenbach JR. Quantitative susceptibility mapping for investigating subtle susceptibility variations in the human brain. Neuroimage 2012;62(3):2083-2100.
19. Liu T, Khalidov I, de Rochefort L, Spincemaille P, Liu J, Tsiouris AJ, Wang Y. A novel background field removal method for MRI using projection onto dipole fields (PDF). NMR Biomed 2011;24(9):1129-1136.
20. Wu B, Li W, Guidon A, Liu C. Whole brain susceptibility mapping using compressed sensing. Magn Reson Med 2012;67(1):137-147.
21. Deistung A, Schweser F, Wiestler B, Abello M, Roethke M, Sahm F, Wick W, Nagel AM, Heiland S, Schlemmer HP, Bendszus M, Reichenbach JR, Radbruch A. Quantitative susceptibility mapping differentiates between blood depositions and calcifications in patients with glioblastoma. PLoS One 2013;8(3):e57924.
22. Bianciardi M, van Gelderen P, Duyn JH. Investigation of BOLD fMRI resonance frequency shifts and quantitative susceptibility changes at 7 T. Hum Brain Mapp 2013.
23. Klohs J, Politano IW, Deistung A, Grandjean J, Drewek A, Dominietto M, Keist R, Schweser F, Reichenbach JR, Nitsch RM, Knuesel I, Rudin M. Longitudinal Assessment of Amyloid Pathology in Transgenic ArcAbeta Mice Using Multi-Parametric Magnetic Resonance Imaging. PLoS One 2013;8(6):e66097.
24. Lim IA, Faria AV, Li X, Hsu JT, Airan RD, Mori S, van Zijl PC. Human brain atlas for automated region of interest selection in quantitative susceptibility mapping: Application to determine iron content in deep gray matter structures. Neuroimage 2013;82C:449-469.
25. Vashaee S, Newling B, MacMillan B, Balcom BJ. B(1) mapping with a pure phase encode approach: quantitative density profiling. J Magn Reson 2013;232:68-75.
26. Wang S, Lou M, Liu T, Cui D, Chen X, Wang Y. Hematoma Volume Measurement in Gradient Echo MRI Using Quantitative Susceptibility Mapping. Stroke 2013;44(8):2315-2317.
27. Liu T, Eskreis-Winkler S, Schweitzer AD, Chen W, Kaplitt MG, Tsiouris AJ, Wang Y. Improved Subthalamic Nucleus Depiction with Quantitative Susceptibility Mapping. Radiology 2013.
28. Kim DH, Choi N, Gho SM, Shin J, Liu C. Simultaneous imaging of in vivo conductivity and susceptibility. Magn Reson Med 2013.
29. Zheng W, Nichol H, Liu S, Cheng YC, Haacke EM. Measuring iron in the brain using quantitative susceptibility mapping and X-ray fluorescence imaging. Neuroimage 2013;78:68-74.
30. Langkammer C, Liu T, Khalil M, Enzinger C, Jehna M, Fuchs S, Fazekas F, Wang Y, Ropele S. Quantitative susceptibility mapping in multiple sclerosis. Radiology 2013;267(2):551-559.
31. Vonken EJ, Schar M, Yu J, Bakker CJ, Stuber M. Direct in vitro comparison of six three-dimensional positive contrast methods for susceptibility marker imaging. J Magn Reson Imaging 2012.
32. Deistung A, Schafer A, Schweser F, Biedermann U, Turner R, Reichenbach JR. Toward in vivo histology: a comparison of quantitative susceptibility mapping (QSM) with magnitude-, phase-, and R2*-imaging at ultra-high magnetic field strength. Neuroimage 2013;65:299-314.

33. Li J, Chang S, Liu T, Wang Q, Cui D, Chen X, Jin M, Wang B, Pei M, Wisnieff C, Spincemaille P, Zhang M, Wang Y. Reducing the object orientation dependence of susceptibility effects in gradient echo MRI through quantitative susceptibility mapping. Magn Reson Med 2012;68(5):1563-1569.
34. Schweser F, Deistung A, Sommer K, Reichenbach JR. Toward online reconstruction of quantitative susceptibility maps: superfast dipole inversion. Magn Reson Med 2013;69(6):1582-1594.
35. Zheng W, Haacke EM, Webb SM, Nichol H. Imaging of stroke: a comparison between X-ray fluorescence and magnetic resonance imaging methods. Magn Reson Imaging 2012;30(10):1416-1423.
36. Cloos MA, Boulant N, Luong M, Ferrand G, Giacomini E, Hang MF, Wiggins CJ, Le Bihan D, Amadon A. Parallel-transmission-enabled magnetization-prepared rapid gradient-echo T1-weighted imaging of the human brain at 7 T. Neuroimage 2012;62(3):2140-2150.
37. Girard OM, Ramirez R, McCarty S, Mattrey RF. Toward absolute quantification of iron oxide nanoparticles as well as cell internalized fraction using multiparametric MRI. Contrast Media Mol Imaging 2012;7(4):411-417.
38. Langkammer C, Schweser F, Krebs N, Deistung A, Goessler W, Scheurer E, Sommer K, Reishofer G, Yen K, Fazekas F, Ropele S, Reichenbach JR. Quantitative susceptibility mapping (QSM) as a means to measure brain iron? A post mortem validation study. Neuroimage 2012;62(3):1593-1599.
39. Li X, Vikram DS, Lim IA, Jones CK, Farrell JA, van Zijl PC. Mapping magnetic susceptibility anisotropies of white matter in vivo in the human brain at 7 T. Neuroimage 2012;62(1):314-330.
40. Liu T, Wisnieff C, Lou M, Chen W, Spincemaille P, Wang Y. Nonlinear formulation of the magnetic field to source relationship for robust quantitative susceptibility mapping. Magn Reson Med 2013;69(2):467-476.
41. Nielsen JF, Hernandez-Garcia L. Functional perfusion imaging using pseudocontinuous arterial spin labeling with low-flip-angle segmented 3D spiral readouts. Magn Reson Med 2013;69(2):382-390.
42. Trujillo-Orrego N, Ibanez A, Pineda DA. [Diagnostic validity of attention deficit/hyperactivity disorder: from phenomenology to neurobiology (II)]. Rev Neurol 2012;54(6):367-379.
43. Gholipour A, Kehtarnavaz N, Scherrer B, Warfield SK. On the accuracy of unwarping techniques for the correction of susceptibility-induced geometric distortion in magnetic resonance Echo-planar images. Conf Proc IEEE Eng Med Biol Soc 2011;2011:6997-7000.
44. Liu T, Xu W, Spincemaille P, Avestimehr AS, Wang Y. Accuracy of the morphology enabled dipole inversion (MEDI) algorithm for quantitative susceptibility mapping in MRI. IEEE Trans Med Imaging 2012;31(3):816-824.
45. Wong R, Chen X, Wang Y, Hu X, Jin MM. Visualizing and quantifying acute inflammation using ICAM-1 specific nanoparticles and MRI quantitative susceptibility mapping. Ann Biomed Eng 2012;40(6):1328-1338.
46. Liu T, Surapaneni K, Lou M, Cheng L, Spincemaille P, Wang Y. Cerebral microbleeds: burden assessment by using quantitative susceptibility mapping. Radiology 2012;262(1):269-278.
47. Denk C, Hernandez Torres E, MacKay A, Rauscher A. The influence of white matter fibre orientation on MR signal phase and decay. NMR Biomed 2011;24(3):246-252.
48. Liu C, Li W. Imaging neural architecture of the brain based on its multipole magnetic response. Neuroimage 2013;67:193-202.
49. Chen WC, Foxley S, Miller KL. Detecting microstructural properties of white matter based on compartmentalization of magnetic susceptibility. Neuroimage 2013;70:1-9.
50. Zhong K, Ernst T, Buchthal S, Speck O, Anderson L, Chang L. Phase contrast imaging in neonates. Neuroimage 2011;55(3):1068-1072.
51. Liu C, Murphy NE, Li W. Probing white-matter microstructure with higher-order diffusion tensors and susceptibility tensor MRI. Front Integr Neurosci 2013;7:11.
52. Lee J, Shmueli K, Kang BT, Yao B, Fukunaga M, van Gelderen P, Palumbo S, Bosetti F, Silva AC, Duyn JH. The contribution of myelin to magnetic susceptibility-weighted contrasts in high-field MRI of the brain. Neuroimage 2012;59(4):3967-3975.
53. Wharton S, Bowtell R. Gradient echo based fiber orientation mapping using r2* and frequency difference measurements. Neuroimage 2013.

54. Wharton S, Bowtell R. Fiber orientation-dependent white matter contrast in gradient echo MRI. Proc Natl Acad Sci U S A 2012;109(45):18559-18564.
55. Wu B, Song B, Tian S, Huo S, Cui C, Guo Y, Liu H. Central nervous system damage due to acute paraquat poisoning: a neuroimaging study with 3.0 T MRI. Neurotoxicology 2012;33(5):1330-1337.
56. Wisnieff C, Liu T, Spincemaille P, Wang S, Zhou D, Wang Y. Magnetic susceptibility anisotropy: cylindrical symmetry from macroscopically ordered anisotropic molecules and accuracy of MRI measurements using few orientations. Neuroimage 2013;70:363-376.
57. Schäfer A, Forstmann BU, Neumann J, Wharton S, Mietke A, Bowtell R, Turner R. Direct visualization of the subthalamic nucleus and its iron distribution using high-resolution susceptibility mapping. Human Brain Mapping 2012;33(12):2831-2842.
58. Schweser F, Deistung A, Lehr BW, Reichenbach JR. Quantitative imaging of intrinsic magnetic tissue properties using MRI signal phase: An approach to in vivo brain iron metabolism? Neuroimage 2011;54(4):2789-2807.
59. Wharton S, Bowtell R. Whole-brain susceptibility mapping at high field: A comparison of multiple- and single-orientation methods. Neuroimage 2010;53(2):515-525.
60. Wu B, Li W, Guidon A, Liu C. Whole brain susceptibility mapping using compressed sensing. Magn Reson Med 2012;67(1):137-147.
61. Li W, Wu B, Batrachenko A, Bancroft-Wu V, Morey RA, Shashi V, Langkammer C, De Bellis MD, Ropele S, Song AW, Liu C. Differential developmental trajectories of magnetic susceptibility in human brain gray and white matter over the lifespan. Hum Brain Mapp 2013.
62. Argyridis I, Li W, Johnson GA, Liu C. Quantitative magnetic susceptibility of the developing mouse brain reveals microstructural changes in the white matter. Neuroimage 2013.
63. Lee J, Shmueli K, Fukunaga M, van Gelderen P, Merkle H, Silva AC, Duyn JH. Sensitivity of MRI resonance frequency to the orientation of brain tissue microstructure. Proc Natl Acad Sci U S A 2010;107(11):5130-5135.
64. Liu C, Li W, Wu B, Jiang Y, Johnson GA. 3D fiber tractography with susceptibility tensor imaging. Neuroimage 2012;59(2):1290-1298.
65. Li W, Wu B, Avram AV, Liu C. Magnetic susceptibility anisotropy of human brain in vivo and its molecular underpinnings. Neuroimage 2012;59(3):2088-2097.
66. Li L, Leigh JS. Quantifying arbitrary magnetic susceptibility distributions with MR. Magnetic Resonance in Medicine 2004;51(5):1077-1082.
67. Haacke EM, Cheng NY, House MJ, Liu Q, Neelavalli J, Ogg RJ, Khan A, Ayaz M, Kirsch W, Obenaus A. Imaging iron stores in the brain using magnetic resonance imaging. Magn Reson Imaging 2005;23(1):1-25.
68. de Rochefort L, Nguyen T, Brown R, Spincemaille P, Choi G, Weinsaft J, Prince MR, Wang Y. In vivo quantification of contrast agent concentration using the induced magnetic field for time-resolved arterial input function measurement with MRI. Med Phys 2008;35(12):5328-5339.
69. Liu T, Spincemaille P, de Rochefort L, Wong R, Prince M, Wang Y. Unambiguous identification of superparamagnetic iron oxide particles through quantitative susceptibility mapping of the nonlinear response to magnetic fields. Magn Reson Imaging 2010;28(9):1383-1389.
70. Liu T, Khalidov I, de Rochefort L, Spincemaille P, Liu J, Tsiouris AJ, Wang Y. A novel background field removal method for MRI using projection onto dipole fields (PDF). NMR Biomed 2011.
71. Liu T, Liu J, de Rochefort L, Spincemaille P, Khalidov I, Ledoux JR, Wang Y. Morphology enabled dipole inversion (MEDI) from a single-angle acquisition: Comparison with COSMOS in human brain imaging. Magnetic resonance in medicine : official journal of the Society of Magnetic Resonance in Medicine / Society of Magnetic Resonance in Medicine 2011.
72. Schweser F, Deistung A, Lehr BW, Reichenbach JR. Differentiation between diamagnetic and paramagnetic cerebral lesions based on magnetic susceptibility mapping. Med Phys 2010;37(10):5165-5178.
73. Schweser F, Lehr BW, Deistung A, Reichenbach JR. A Novel Approach for Separation of Background Phase in SWI Phase Data Utilizing the Harmonic Function Mean Value Property. Proc ISMRM 2010:142.
74. Wharton S, Bowtell R. Whole-brain susceptibility mapping at high field: a comparison of multiple- and single-orientation methods. Neuroimage 2010;53(2):515-525.

75. Wharton S, Schafer A, Bowtell R. Susceptibility mapping in the human brain using threshold-based k-space division. Magn Reson Med 2010;63(5):1292-1304.
76. Haacke EM, Tang J, Neelavalli J, Cheng YC. Susceptibility mapping as a means to visualize veins and quantify oxygen saturation. J Magn Reson Imaging 2010;32(3):663-676.
77. Wu B, Li W, Guidon A, Liu C. Whole brain susceptibility mapping using compressed sensing. Magn Reson Med 2011.
78. Liu J, Liu T, de Rochefort L, Ledoux J, Khalidov I, Chen W, Tsiouris AJ, Wisnieff C, Spincemaille P, Prince MR, Wang Y. Morphology enabled dipole inversion for quantitative susceptibility mapping using structural consistency between the magnitude image and the susceptibility map. Neuroimage 2012;59(3):2560-2568.
79. Liu T, Xu W, Spincemaille P, Avestimehr AS, Wang Y. Accuracy of the Morphology Enabled Dipole Inversion (MEDI) Algorithm for Quantitative Susceptibility Mapping in MRI. Ieee T Med Imaging 2012;31(3):816-824.
80. Bilgic B, Pfefferbaum A, Rohlfing T, Sullivan EV, Adalsteinsson E. MRI estimates of brain iron concentration in normal aging using quantitative susceptibility mapping. Neuroimage 2012;59(3):2625-2635.
81. Liu T, Wisnieff C, Lou M, Chen W, Spincemaille P, Wang Y. Nonlinear formulation of the magnetic field to source relationship for robust quantitative susceptibility mapping. Magnetic resonance in medicine : official journal of the Society of Magnetic Resonance in Medicine / Society of Magnetic Resonance in Medicine 2012.
82. Lotfipour AK, Wharton S, Schwarz ST, Gontu V, Schafer A, Peters AM, Bowtell RW, Auer DP, Gowland PA, Bajaj NP. High resolution magnetic susceptibility mapping of the substantia nigra in Parkinson's disease. Journal of magnetic resonance imaging : JMRI 2012;35(1):48-55.